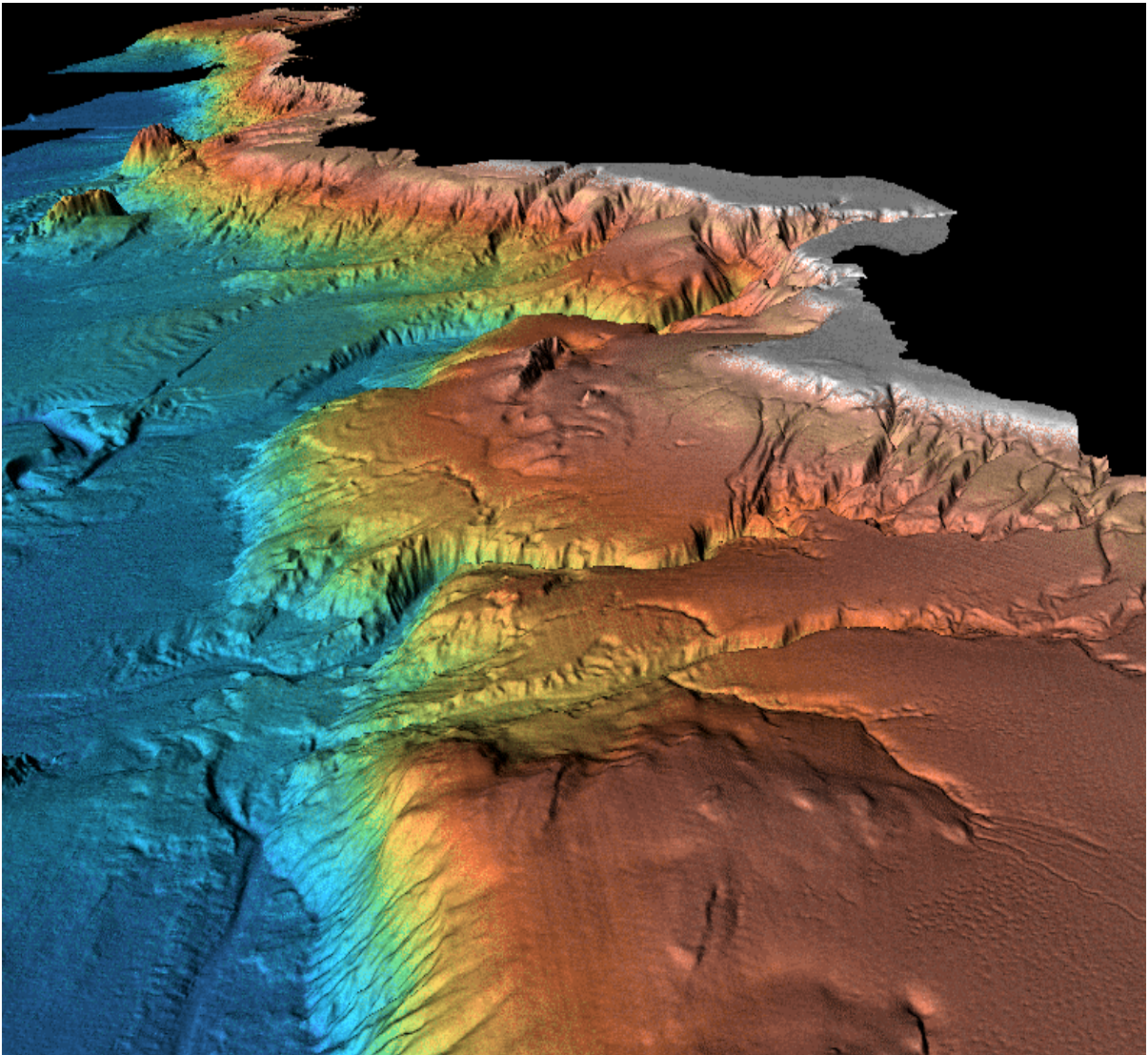


The California Current System: Comparison of Geostrophic Currents, ADCP Currents and Satellite Altimetry



**LCDR David O. Neander, NOAA
OC3570 Summer Cruise, August 2-5, 2001**

I. INTRODUCTION

The large-scale atmospheric forcing in the eastern Pacific Ocean consists of the North Pacific (sub-tropical) high, the Aleutian low, and in summer the thermal low over the western United States. The North Pacific High is most intense during the summer months while the Aleutian low is most intense during the winter months. During summer months, the thermal low enhances equatorward wind stress over the coastal waters off northern California. These forces act to create the anticyclonic North Pacific Subtropical Gyre, which includes the North Equatorial Current (NEC), Kuroshio Current, North Pacific Current (West Wind Drift) and the California Current System.

The California Current System (CCS) forms the eastern limb of the North Pacific Subtropical Gyre, flowing equatorward off the western United States and northern Mexico. The CCS is a classic eastern ocean coastal upwelling system with a narrow to moderate continental shelf and generally broad, diffuse, equatorward surface flow (Parrish et al., 1983). From the Strait of Juan de Fuca to Point Conception, the CCS has traditionally been divided into three large-scale (> 500 km) alongshore currents: the California Current (CC), the Davidson Current (DC), and the California Undercurrent (CUC) (Hickey, 1998). The CC is a surface (0-300 m deep) current, which carries colder, fresher subarctic water equatorward throughout the year with average speeds generally less than 25 cm s^{-1} (Reid and Schwartzlose, 1962). Thus, the CC is characterized by a low salinity, low temperature core which usually lies between 300-400 km offshore (Lynn and Simpson, 1987). The CUC flows poleward over the continental slope from Baja to at least 50° N with a relatively narrow width between 10-40 km (Hickey, 1998). The CUC has its origin in the eastern equatorial Pacific, and is identified by its warm, saline, oxygen and nutrient-poor signature. Hickey (1979) concluded that the location, strength and core depth show considerable seasonal variability and can be related to the seasonal variability in wind stress and curl of the wind stress. Peak speeds of the undercurrent are about $30\text{-}50 \text{ cm s}^{-1}$ being stronger at depths of 100-300 m and can be continuous over distances of more than 400 km along the slope (Collins et al., 1996). The DC is a seasonal current, flowing poleward at the surface during the fall and winter over the shelf from Point Conception to Vancouver Island. Measurements in the region

have shown that the seasonal cycle over the slope is highly variable with the poleward flow maximum usually occurring in May (Collins et al., 1996). The reversal of winds from northwesterly in summer to southeasterly in winter, which causes downwelling at the coast, seems to be the forcing mechanism of this poleward surface current (Huyer et al., 1989). It has been suggested that the DC is a result of the “surfacing” of the CUC during late fall (Pavlova, 1966; Huyer and Smith, 1974).

In addition to the CC, CUC and DC, sea surface height from altimeter data and satellite images of sea surface temperature and ocean color have revealed a complex structure of mesoscale features such as jets, filaments and eddies superimposed on the slow, generally southward flow.

II. PURPOSE

The purpose of this report is to compare computed geostrophic currents calculated from 35 conductivity, depth, pressure (CTD) casts, with currents measured by an Acoustic Doppler Current Profiler (ADCP). This data will also be compared to real-time satellite imagery, the TOPEX/ERS-2 sea surface height anomaly. In addition, geostrophic velocities will be used to compute volume transport in and out of the “CenCal Box” formed by the CTD sampling scheme.

III. PROCEDURE

A. Data Collection

CTD and ADCP data were acquired along California Cooperative Oceanic Fisheries Investigation (CalCOFI) line 67 (stations 9-18), along a CalCOFI “70s” alongshore line (stations 19-29) and along CalCOFI line 77 (stations 30-43) aboard the R/V POINT SUR from August 2-5, 2001. Locations of stations 9-43 are depicted in Figure 1. Data were acquired at each station using a Sea-Bird Electronics, Inc. CTD, which provided continuous measurements of conductivity (which provided salinity), temperature and pressure. All CTD casts were taken to a pressure of 1000 dbar or near bottom (whichever came first), except at station 26, where a full depth (3965 dbar) cast

was acquired. The vessel mounted ADCP measured currents along the ship's track. This data was processed as north-south and east-west components, and rotated approximately 30° to correspond to actual across line and along line velocities.

B. Calculations

Geostrophic velocities were calculated from the CTD data using the SEAWATAER library of MATLAB routines supplied by the Commonwealth Scientific and Industrial Research Organization (CSIRO). Following the guidelines of Pond and Pickard (1983), geostrophic velocity is calculated as follows:

$$f\mathbf{v} = \frac{-1}{\rho} \frac{\partial \mathbf{p}}{\partial \mathbf{x}}$$

or

$$\mathbf{v} = \frac{-1}{f\rho} \frac{\partial \mathbf{p}}{\partial \mathbf{x}}$$

where:

ρ = density

f = Coriolis = $2\Omega \sin \varphi$

Ω = angular speed of rotation of the earth = $7.292 \times 10^{-5} \text{ s}^{-1}$

φ = latitude

$\frac{\partial \mathbf{p}}{\partial \mathbf{x}}$ = pressure gradient along line between CTD casts

Two practical forms of the geostrophic equation:

$$(V_1 - V_2) = \frac{1}{L 2\Omega \sin\phi} \left[\int \delta_B dp - \int \delta_A dp \right]$$

or:

$$(V_1 - V_2) = \frac{1}{L 2\Omega \sin\phi} \left[\Delta\Phi_B - \Delta\Phi_A \right]$$

using mixed units:

$$(V_1 - V_2) = \frac{10}{L 2\Omega \sin\phi} \left[\Delta D_B - \Delta D_A \right]$$

where:

L = distance between stations A and B

δ = specific volume anomaly

dp = pressure difference

$\Delta\Phi$ = geopotential anomaly

$\Delta D = \int \delta dp$ (geopotential distance, integrated from the surface to a level of no motion)

hence:

$$v = \frac{\Delta D}{L 2\Omega \sin\phi}$$

This calculates geostrophic velocity perpendicular to the line between the two CTD stations, equivalent to the rotated “across” line velocities computed from the ADCP data.

For most stations, geostrophic velocities relative to 1000 dbar were calculated. However, at those stations where the depth of the bottom is less than 1000 m, a reference level of 1000 dbar is not available. For 11 such stations, CTD9 and CTD34-43, the surface flow was estimated by extrapolating the offshore horizontal density gradient at levels between the deepest observed levels at these stations and 1000 dbar.

IV. RESULTS AND DISCUSSION

A. Synoptic Evaluation

1. Satellite Altimetry

Figure 2 depicts the sea surface height anomaly for 5 August 2001. This image was derived from TOPEX and ERS-2 satellite altimeter data and downloaded from the Global Near Real-Time Sea Surface Height Data Viewer of the Colorado Center for Astrodynamic Research (CCAR) (http://www-ccar.colorado.edu/~realtime/global-real-time_ssh/). Within this image, four distinct features are evident in relation to the overlaid tracks of CalCOFI line 67, 70s line and line 77: a high (> 2 cm) centered north of line 67; a low (< 3 cm) centered southeast of line 67; a low (< 4 cm) centered west of line 67 and the 70s line; a high (> 3 cm) centered on line 77. The resulting flow from these features is clockwise around highs (“light on right”) and counter-clockwise around lows.

2. T-S Diagrams

CalCOFI Line 67

The T-S diagram of Figure 3 depicts cooler, saline surface water most likely associated with coastal upwelling and equatorward flow of cool, fresh arctic waters characteristic of the California Current. There is also a distinct separation between two water masses. The cool, fresher waters of the California Current can be distinguished from the warmer, saline waters of the California Undercurrent. This separation becomes readily apparent below ~ 100 dbar (or $\sim 10^\circ$ C).

CalCOFI 70s Line

The T-S diagram of Figure 3 depicts significant variations in temperature and salinity in the upper 100 dbar. Below this level the water column is well mixed, and water masses of different origins are not recognizable. Variations in the upper water column and significant mixing below are an indication that the structure of the entire

water column is very complex, which is consistent with the transition zone of the California Current. Lynn and Simpson (1987) hypothesize that recurrent mesoscale eddies and energetic meanders create this zone.

CalCOFI Line 77

The T-S diagram of Figure 3 indicates significantly more upper level mixing than was shown for line 67. This is most likely due to the fact that the continental slope extends further offshore along line 77, and includes the Santa Lucia Escarpment and the Santa Lucia Bank. These bathymetric features tend to increase mixing in the upper 500 dbar, in part due to interactions of upwelling and the California Undercurrent, as well as by solitary internal waves (solitons) generated at the shelf break by the interaction of the M2 tide with the bottom slope. These baroclinic or internal tides may propagate onto the shelf and enhance mixing (Lien and Gregg, 2001).

Below ~ 200 dbar (9° C), there is a distinct separation between water masses, as with line 67. Specifically, the cool, fresh waters of the California Current can be separated from the warm, saline waters of the California Undercurrent. This distinction is readily apparent in the 1000 dbar temperature profile of Figure 12.

B. Comparisons

1. Sea Surface Height Anomaly vs. ADCP Currents

CalCOFI Line 67

Three features in Figure 2 are evident along the track of line 67: a high (> 2 cm) centered north of the track, a low (< 3 cm) centered southeast of the track and a low (< 4 cm) centered west and south of the track. The low centered offshore of line 67 results in a weak poleward flow of warm water across the western 1/3 of line 67, which is evident in the upper layer across track ADCP velocities shown in Figures 4 and 5. The high north of the track and the low southwest of the track would result in an offshore flow near the coast, which is indicative of coastal upwelling. Upwelling is evident in the

ADCP along track velocity profile (Figure 6). The California Undercurrent, which transports warm, saline water poleward is clearly visible in the ADCP across track profile (Figure 5). The California Undercurrent is not evident in the TOPEX/ERS-2 data along line 67.

CalCOFI 70s Line

One major feature in Figure 2 is evident along the track of the 70s line: a low (< 4 cm) centered west of the track. This counter-clockwise flow around the low results in weak poleward flow along the northern half of the track. This is evident in the ADCP along track velocity of Figures 4 and 6, which show weak poleward flow northward from 35.5° N.

CalCOFI Line 77

One significant feature in Figure 2 is readily apparent along the track of line 77: a high (> 3 cm) is centered on the track near 121.3° W. The resulting flow from this feature is poleward from 121.3° to 122° W, and equatorward from 121.25° W inshore. This poleward flow, characteristic of the CUC, is evident in the ADCP across track profile (Figure 5). The nearshore equatorward flow is not evident in either the ADCP “stick” plot (Figure 4) nor the ADCP across track plot (Figure 5), perhaps due to the characteristics of the shallow, well mixed water.

2. Sea Surface Height Anomaly vs. CTD Data

CalCOFI Line 67

Figures 7 and 10 depict the salinity, temperature and density anomaly sections for the CTD data (300 dbar and 1000 dbar, respectively). Two near-surface features are apparent in these figures. The first, upwelling of cool, saline waters is visible in the nearshore profile (vicinity of 122.2° W). The second feature, located near the surface in the offshore section (vicinity of 123.3° W) consists of warmer, less saline waters. This high temperature, fresh water is most likely attributed to the California Current’s

equatorward transport of subarctic waters mixing with warm water resulting from surface heating and advection of warmer waters from the south. Below 80 dbar, in the vicinity of 122.2° W a distinct change of water properties is apparent, specifically the high temperature and salinity characteristics of the CUC. The CUC is not evident in the satellite altimetry data across line 67.

The temperature and salinity parameters are combined within MATLAB using the CSIRO SEAWATER routines, to produce the density anomaly. A low density anomaly is depicted offshore, corresponding to a high temperature and low salinity signature. Considering that low density corresponds to a high sea surface height anomaly, one would expect to see a higher sea surface height than what is actually shown in the satellite altimetry data. This may be due to the resolution of the satellite altimeter, or the weak gradients in sea surface height along the offshore edge of line 67. As a result of upwelling, the isopycnals slope upward towards shore, corresponding to a low temperature, high salinity signature. This in turn corresponds to a low sea surface height, evident in Figure 2. The decrease in density associated with the CUC is not evident in Figure 2. The most rapid change in slope of the isopycnals occurs in the vicinity of 122.7° W, which corresponds to strong horizontal temperature gradients.

CalCOFI 70s Line

Figures 8 and 11 depict the temperature and salinity sections for the CTD data (300 dbar and 1000 dbar, respectively). In the upper 25 m, there is little variation in temperature and salinity; hence there is minimal variation in the upper 25 m density anomaly. However, two noteworthy features below 25 m depth deserve some discussion. The first is a strong bowing down of the isotherms at 40-80 m depths, in the vicinity of 35.1° N. This feature is clearly evident in the density anomaly profile, which shows a decrease in density anomaly associated with the downwelling of warm surface waters. The second feature is the upwelling of cool, saline water in depths ranging from 30-150 m, in the vicinity of 36° N. This is also evident in the density anomaly profile, which shows an increase in the density anomaly, corresponding to a decrease in temperature and increase in salinity. This strong gradient in density to the north corresponds to a lower

sea surface height as depicted in Figure 2. These features appear to be located near the transition zone of the California Current, where mesoscale eddies and energetic meanders are common.

CalCOFI Line 77

Figures 9 and 12 depict the temperature and salinity sections for the CTD data (300 dbar and 1000 dbar, respectively). Two near-surface features are apparent in these figures. The first, upwelling of cool, saline waters along the slope is evident in the vicinity of 120.9° W. The upwelling of cool, saline water corresponds to an increase in density anomaly along the slope. The second near-surface feature, located offshore in the vicinity of 122.1° W consists of warmer, less saline waters. This high temperature, fresh water characterized by a low density anomaly, which corresponds to a high sea surface height anomaly. This feature is confirmed in Figure 2, which depicts a ~ 4 cm high centered on line 77.

Upon inspection of the subsurface temperature and salinity profiles (Figures 9 and 12), the intrusion of the California Undercurrent is revealed in the vicinity of 121.4° W. As previously stated the undercurrent is characterized by warm, saline waters, which flow poleward along the slope at depths of 100-300 m. This warm, saline water results in a decrease in the density anomaly (Figure 12).

One of the more striking features along line 77 is the strong gradient in temperature and salinity in the vicinity of 121.2° W. This feature has the appearance of an upwelling event, with cooler, saline water pushed toward the surface. Upon inspection of the local bathymetry, this event transpires over the Santa Lucia Escarpment. This low temperature and low salinity feature is most likely associated with upwelling along the escarpment or non-linear interactions of the M2 tide with the offshore slope of the escarpment.

3. CTD calculated geostrophic currents vs. ADCP measured currents

CalCOFI Line 67

Calculated geostrophic velocities are depicted in Figure 7 and Figure 10, to a depth of 300 dbar and 1000 dbar, respectively. These figures show alternating equatorward and poleward flow with significant variations above 500 dbar, while variations below 500 dbar are less than 5 cm s^{-1} . Comparing the upper 300 dbar geostrophic currents with ADCP measured currents (Figures 4 and 5), there is a general correlation in the poleward flow at 122.6° W , which is characteristic of the California Undercurrent. The calculated geostrophic velocities show a much greater variation in poleward and equatorward flow, which can be related to the upper 300 dbar density anomaly profile of Figure 7. Density anomaly gradients represent poleward or equatorward flow, with maximums and minimums appearing to represent zero velocities at inflection points. The offshore variations in poleward and equatorward flow may be attributed to the transition zone of the California Current, which contains a complex system of meanders, filaments, submesoscale and mesoscale eddies.

CalCOFI 70s Line

Calculated geostrophic velocities are depicted in Figure 8 and Figure 11, to a depth of 300 dbar and 1000 dbar, respectively. These figures show alternating east-west flow (west being “+”), with significant variations above 500 dbar while variations below 500 dbar are less than $\pm 5 \text{ cm s}^{-1}$. Comparing the upper 300 dbar geostrophic currents with ADCP measured currents (Figures 4 and 5), there is little correlation between the across track flow. Again the calculated geostrophic velocities show a much greater variation in across track flow, and can be related to the upper 300 dbar density profile of Figure 8. These offshore variations are most likely attributed to the transition zone of the California Current.

CalCOFI Line 77

Calculated geostrophic velocities are depicted in Figure 9 and Figure 12, to a depth of 300 dbar and 1000 dbar, respectively. These figures show alternating equatorward and poleward flow with significant variations above 500 dbar, while variations below 500 dbar are less than 5 cm s^{-1} . Comparing the upper 300 dbar geostrophic currents with ADCP measured currents (Figures 4 and 5), there is a general correlation in the poleward flow in the vicinity of 121.6° W , which is characteristic of the California Undercurrent. Both the calculated geostrophic velocities and measured ADCP velocities show significant variations in poleward and equatorward flow. Line 77 crosses an area of complex bottom topography, in particular the Santa Lucia Escarpment and the Santa Lucia Bank. These bathymetric features are most likely responsible for the variations in flow, in part due to upwelling events and internal waves of tidal frequency.

4. Volume Transport

The principle of conservation of volume (or the equation of continuity) follows from the fact that the compressibility of water is small, and that if water is flowing into a closed, full container at a certain rate it must be flowing out somewhere else at the same rate (Pickard and Emery, 1990). Assuming the “container” is the CenCal box formed by CalCOFI line 67, 70s line and line 77, the volume transport “into” and “out of” the box should be conserved. Knowing the distance between each station (L), vertical (depth) limits (dz), and the geostrophic velocity normal to the line joining the two stations relative to a reference level ($v - v_r$), determination of the volume transport (V_T) is relatively straightforward.

$$V_T = L \int (v - v_r) dz$$

Averaging the geostrophic velocity over the upper 300 dbar or maximum cast depth (stations CTD9 and CTD 40-43), the volume transports for each line were computed in $\text{m}^3 \text{ s}^{-1}$ and converted to Sverdrups ($1 \text{ Sv} = 10^6 \text{ m}^3 \text{ s}^{-1}$). Figure 13 shows the details of the volume transport calculations across each line.

To summarize:

North transport on CalCOFI line 77 (“into box”):	+ 1.81 Sv
North transport on CalCOFI line 67 (“out of box”):	- 1.35 Sv
West transport on 70s CalCOFI line (“out of box”):	<u>- 0.29 Sv</u>
Difference between volume transport “into and out of CenCal Box”:	+ 0.17 Sv

V. CONCLUSIONS

Variations in the physical characteristics and large-scale current patterns of the California Current System were evident in the CTD data, ADCP currents and TOPEX/ERS-2 satellite altimetry. In a broad sense, the geostrophic velocity field, ADCP currents and satellite altimetry were in general agreement. However, notable differences were observed during the comparisons.

The core of the California Undercurrent was evident in both CTD and ADCP data along the slope at depths of 100-400 m, while the satellite imagery only indicated the undercurrent on line 77. Significant variations in poleward and equatorward flow were noted in the geostrophic velocities along lines 67 and 77, apart from the CUC. The complexity of the physical characteristics noted in the CTD data is related to vertical adjustments in the water column caused by intrusions of waters from different sources. Upwelling events, along with internal waves generated at the shelf break contribute to these variations in density, which in turn controls the strength and direction of the geostrophic flow.

The California Current, defined as a surface (0-300 m deep) current transporting cold, fresher subarctic water equatorward was not clearly identified. The core of the CC, usually 300-400 km offshore, was beyond the range of our sampling scheme. However, the transition zone of the CC, located approximately 200 km offshore became evident within the CTD and ADCP data, as well as the satellite imagery. Cores of low salinity and high velocity were observed, which correspond to meanders of the CC, a characteristic of the transition zone.

Volume transports across each line were calculated using the upper 300 dbar depth averaged geostrophic velocities. The net transport, +0.17 Sv, was the remaining transport in the box formed by the sampling grid. According to the conservation of volume principle, there must be 0.17 Sv flowing out elsewhere. Since only the upper 300 dbar depth averaged velocities were used in the volume transport computation, one could hypothesize that the remaining outflow occurs in the layers below 300 dbar.

The complex characteristics of the California Current System have been extensively studied over the past 50+ years, yet even today we find new evidence of seasonal variations. No single study or combined group of studies can completely describe the variations in physical characteristics and current patterns in this unique eastern boundary current.

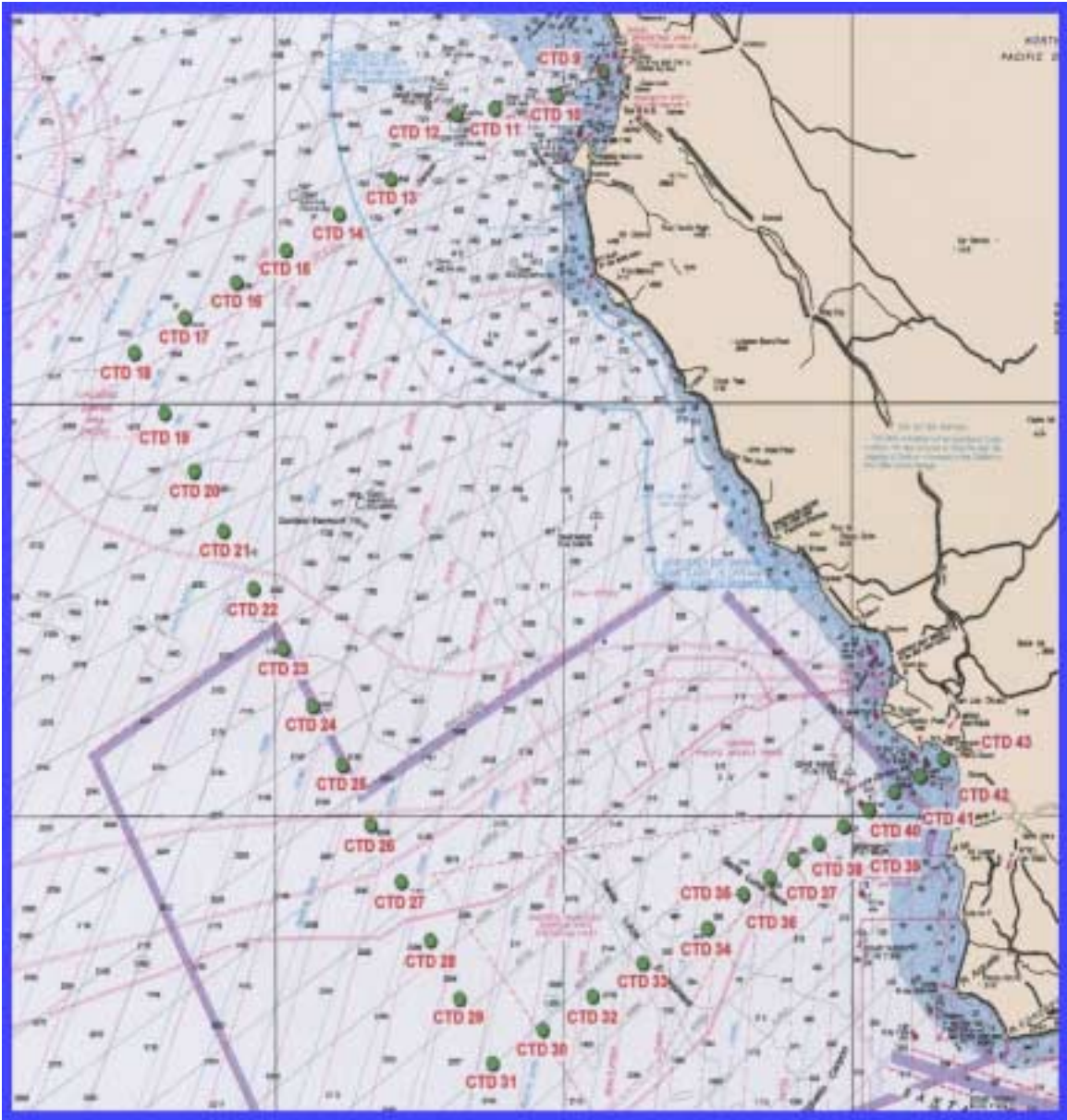


Figure 1
Station Locations

TOPEX/ERS-2 Analysis Aug 5 2001

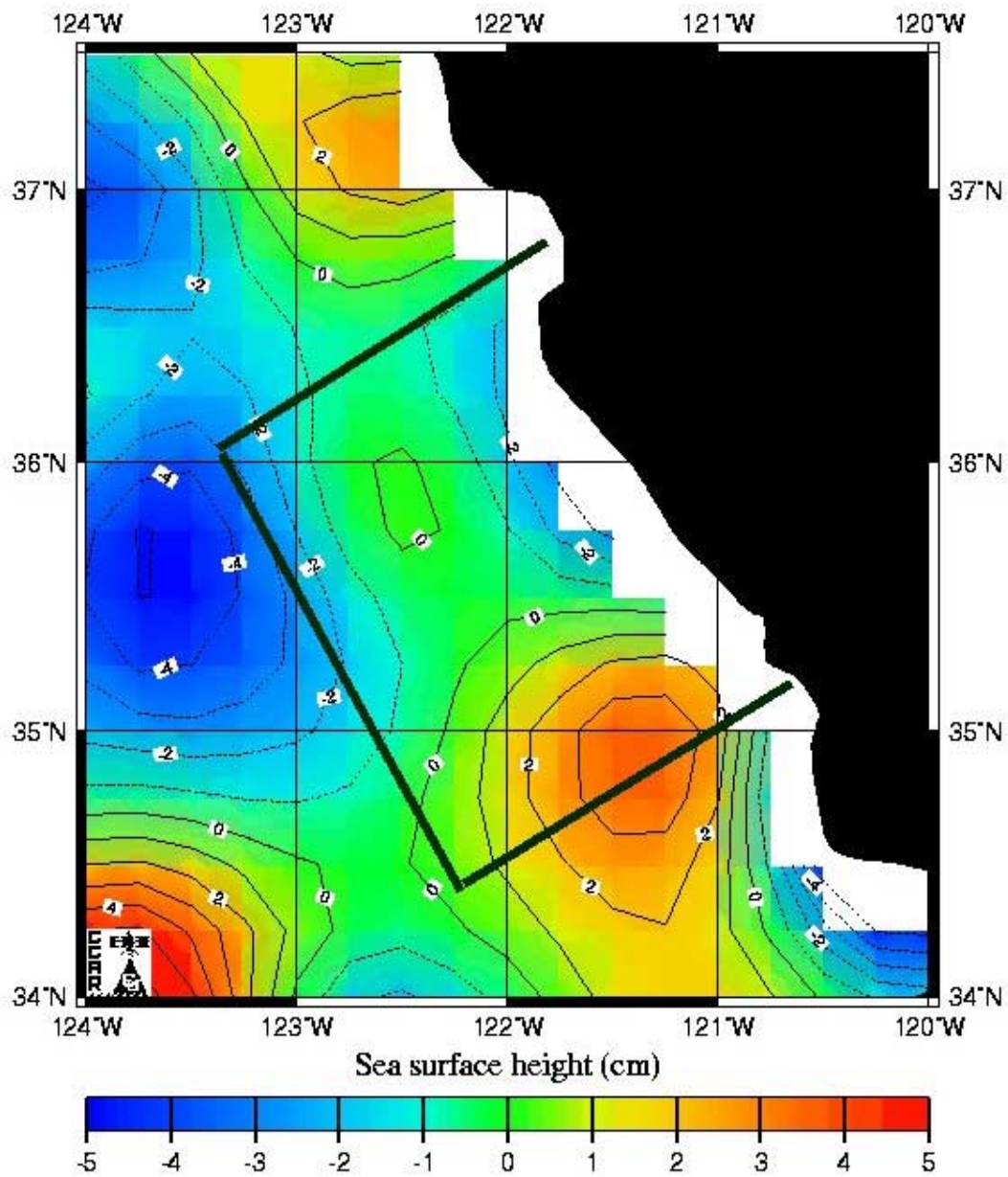


Figure 2
Satellite Altimetry

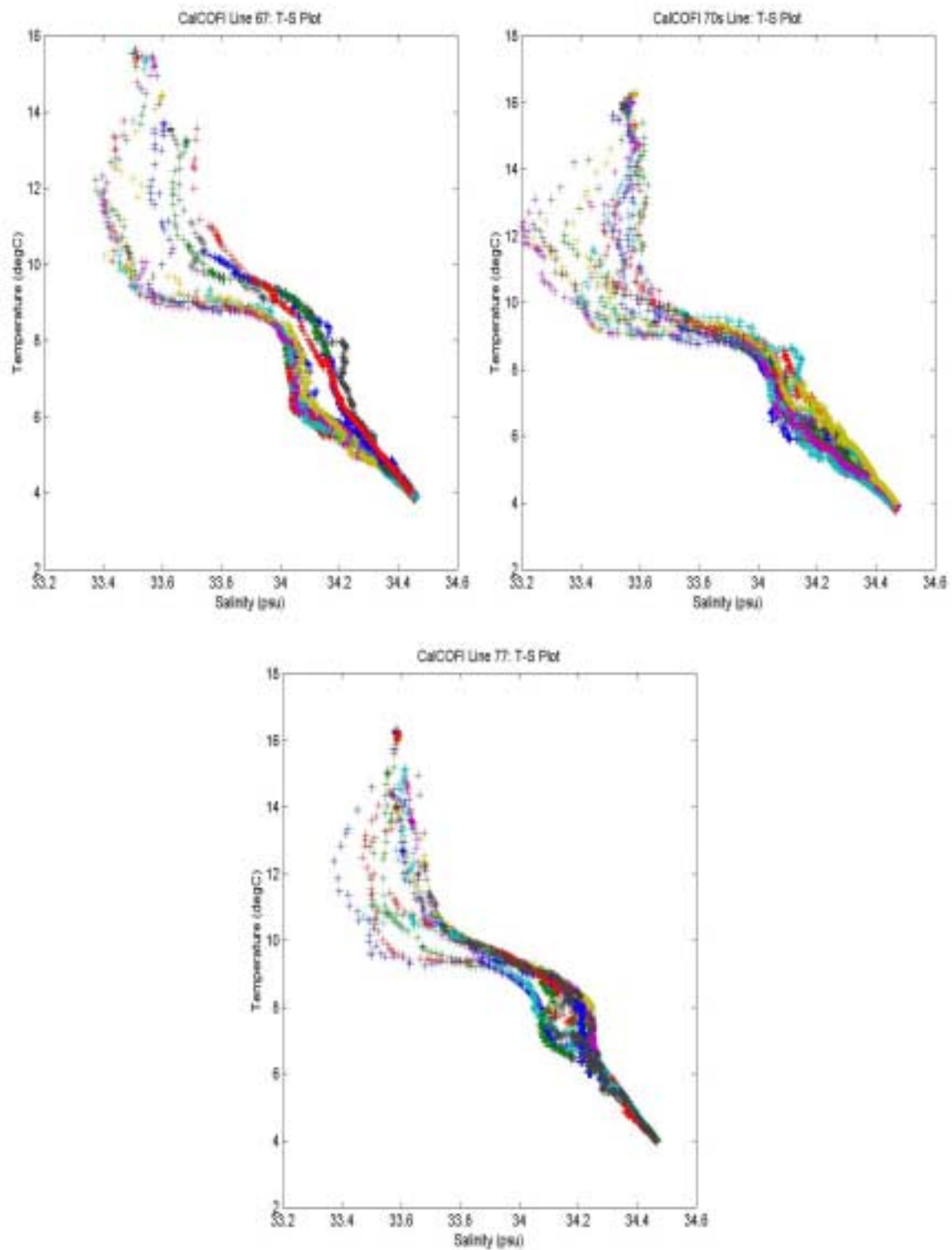


Figure 3
T-S Diagrams

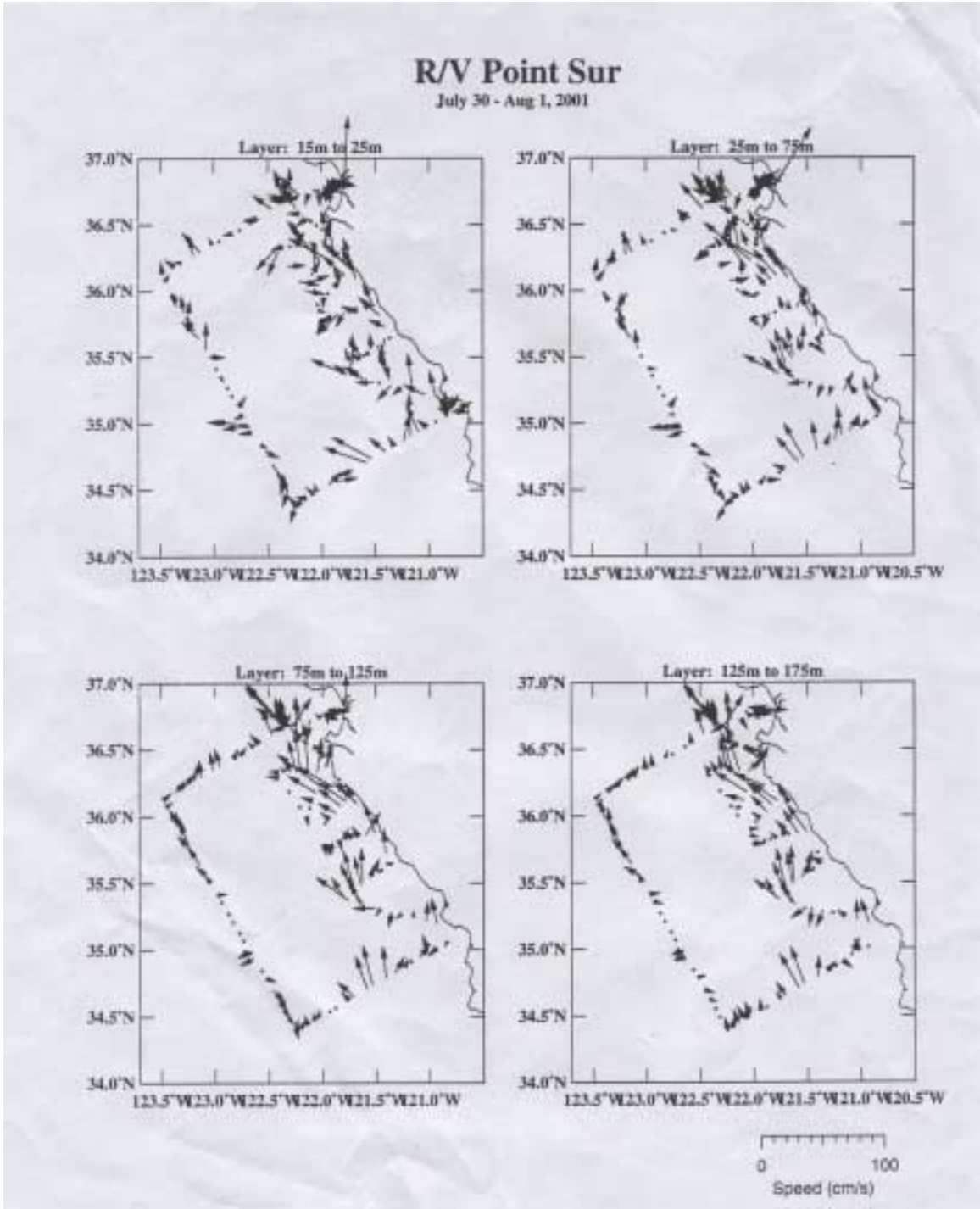


Figure 4
ADCP Velocities

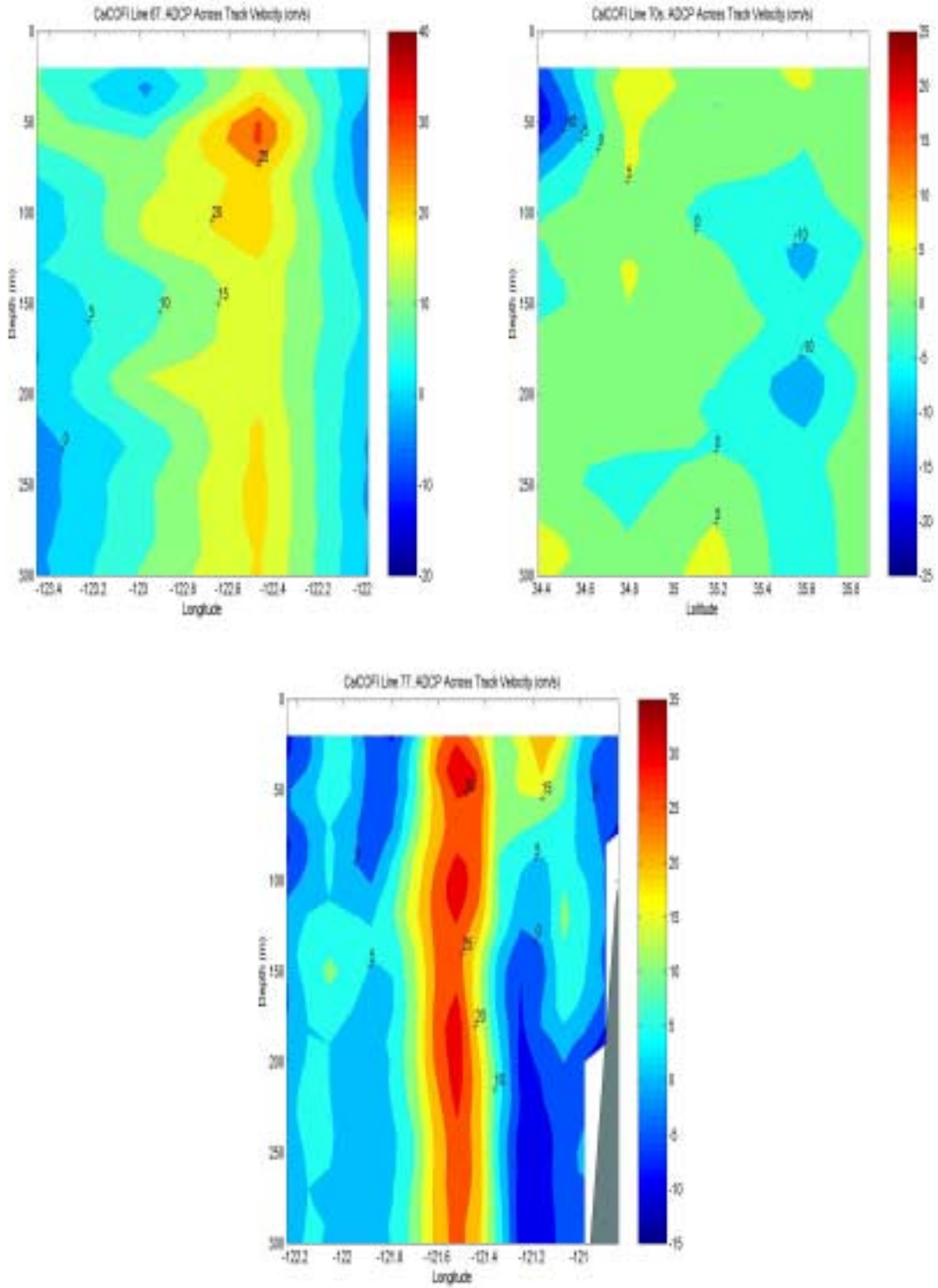


Figure 5
ADCP Across Track Velocity

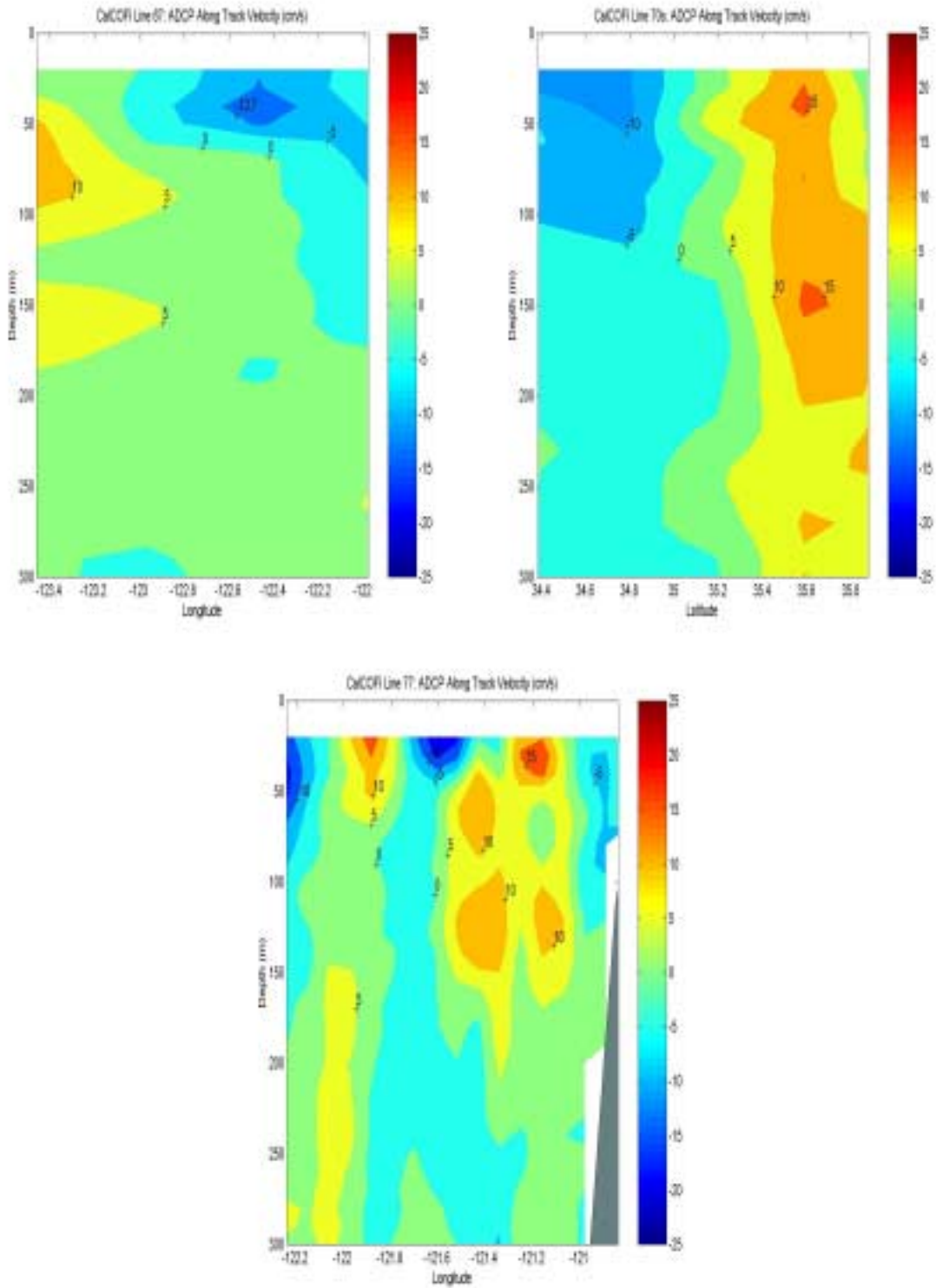


Figure 6
ADCP Along Track Velocity

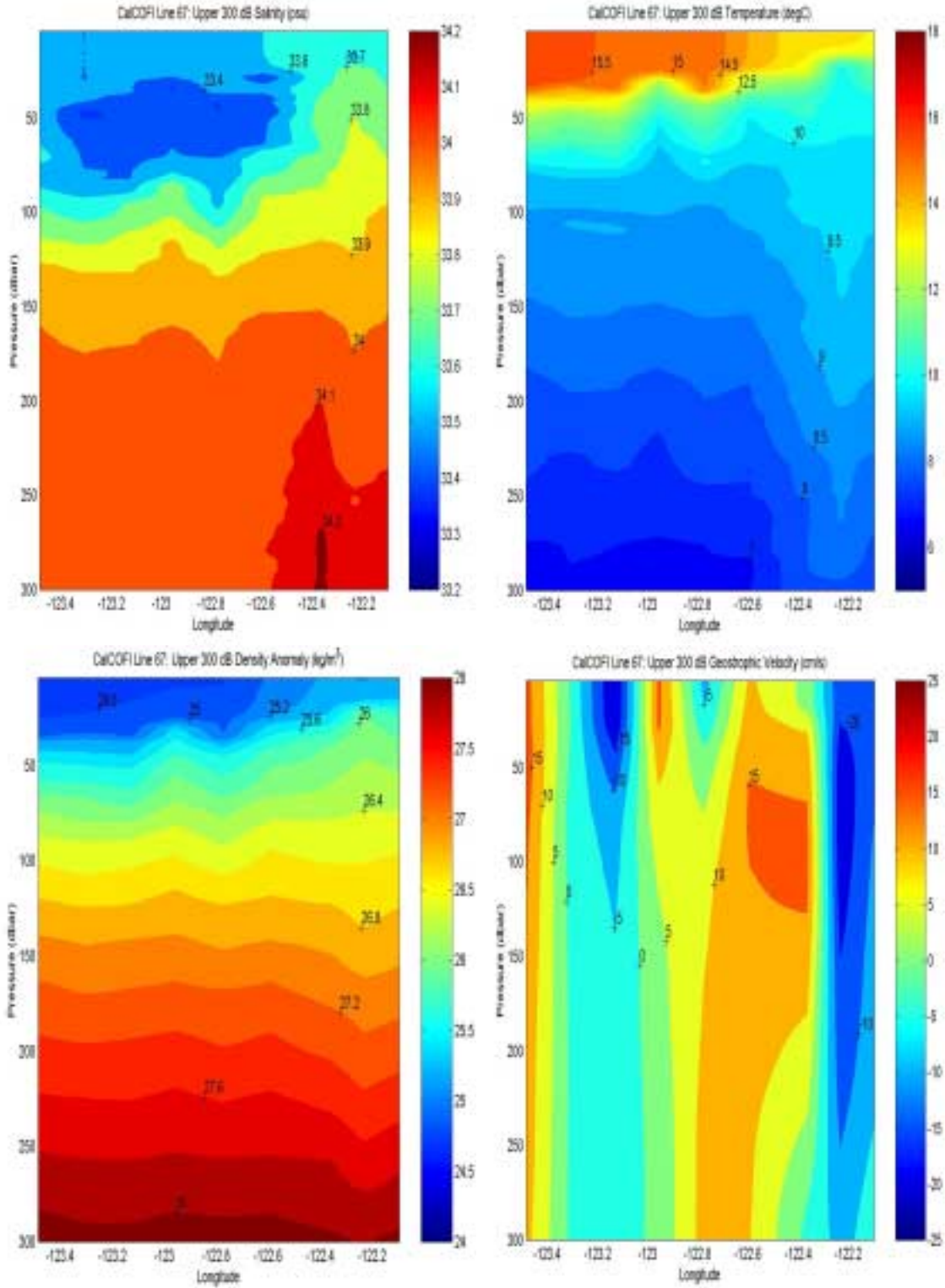


Figure 7
CalCOFI Line 67 – Upper 300 dbar

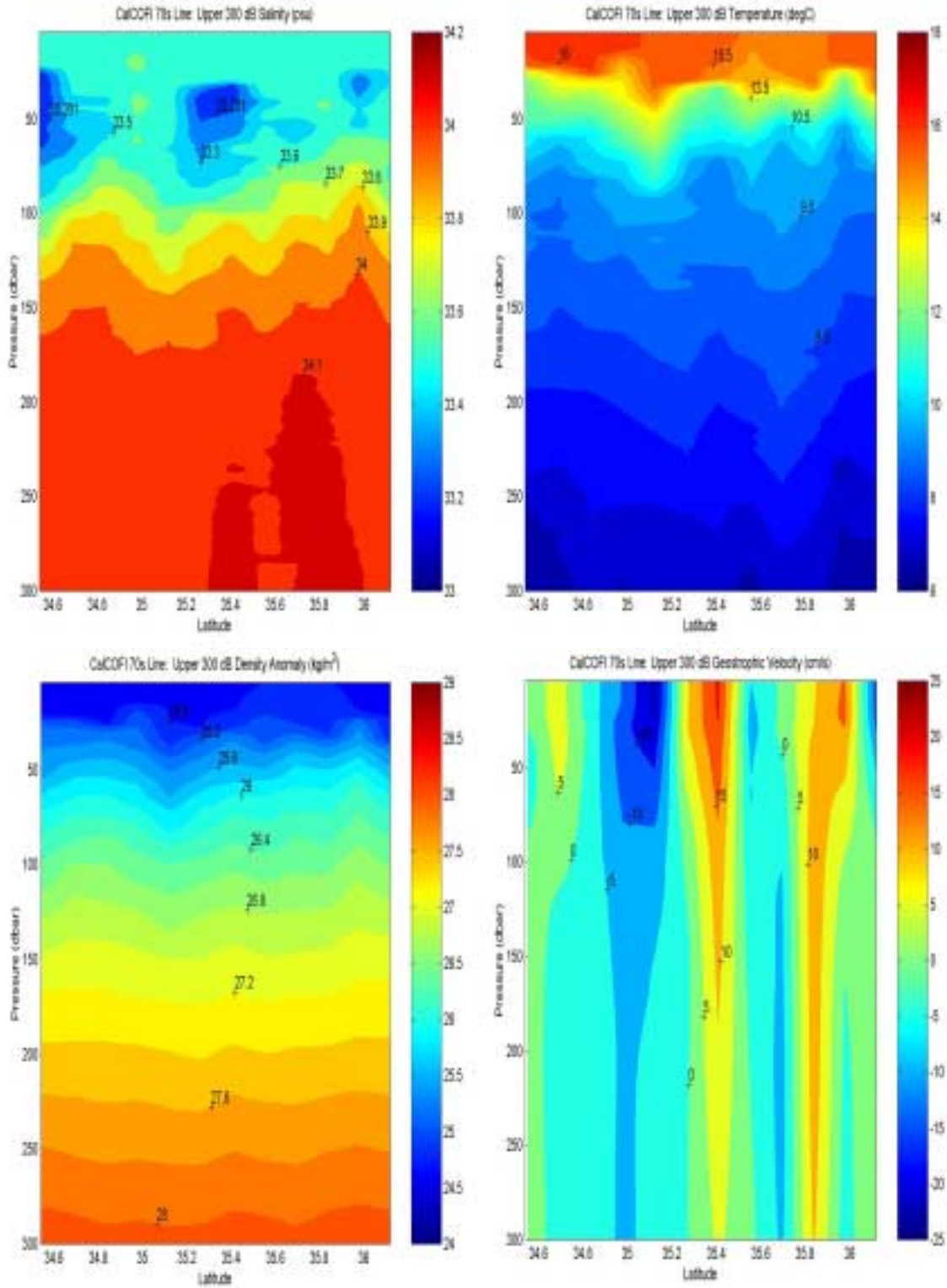


Figure 8
CalCOFI 70s Line – Upper 300 dbar

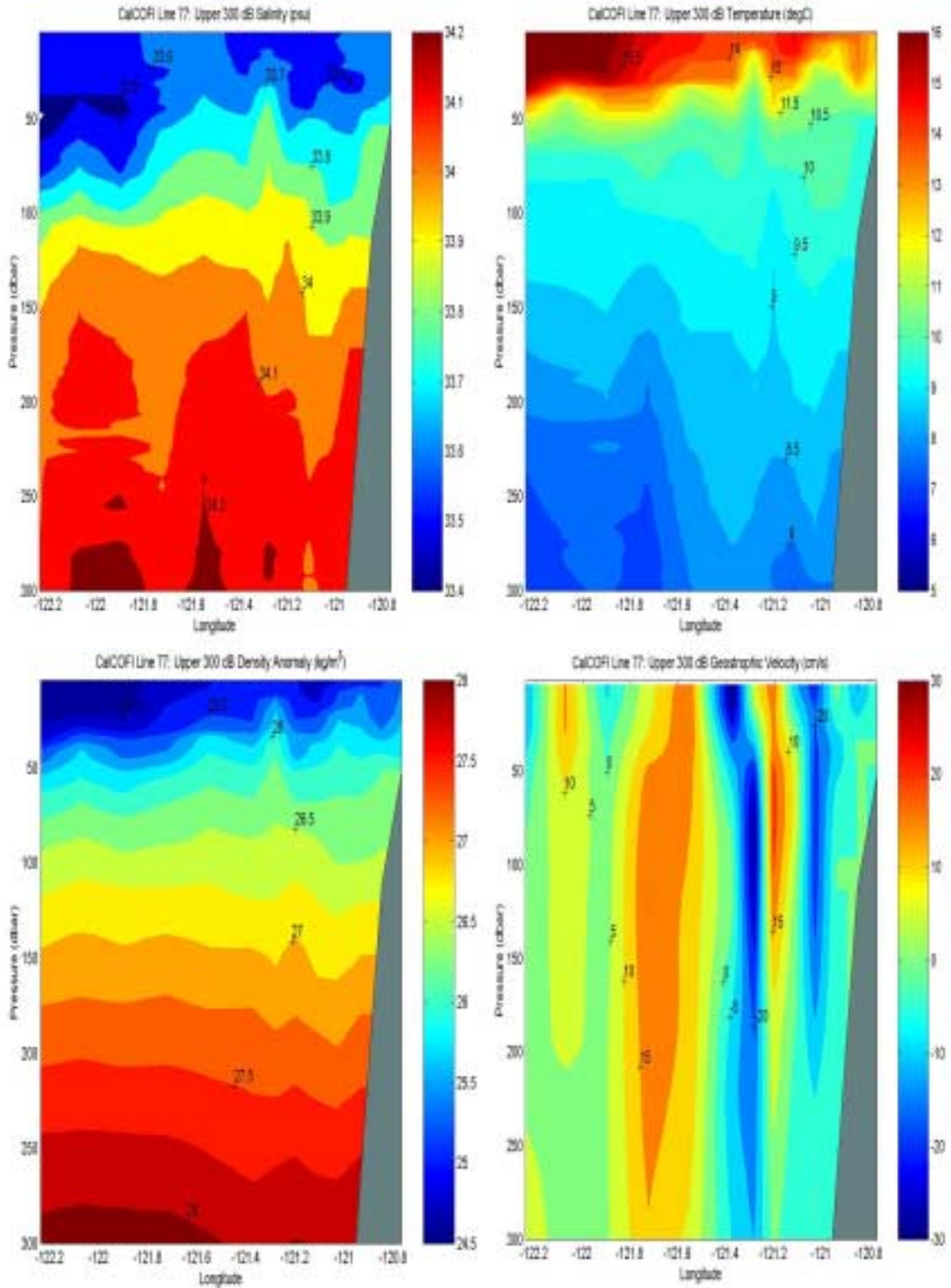


Figure 9
CalCOFI Line 77 – Upper 300 dbar

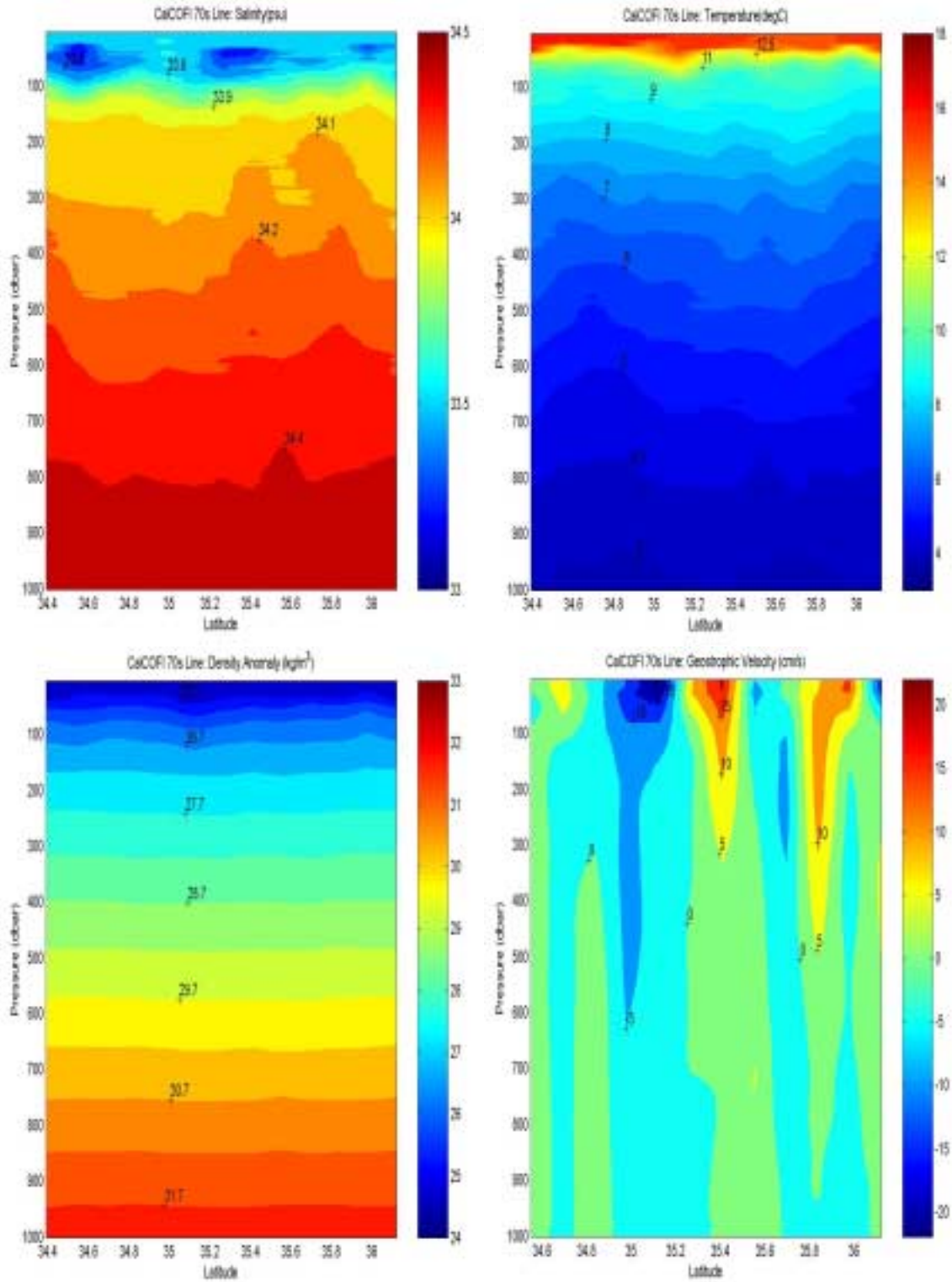


Figure 11
CalCOFI 70s Line – 1000 dbar

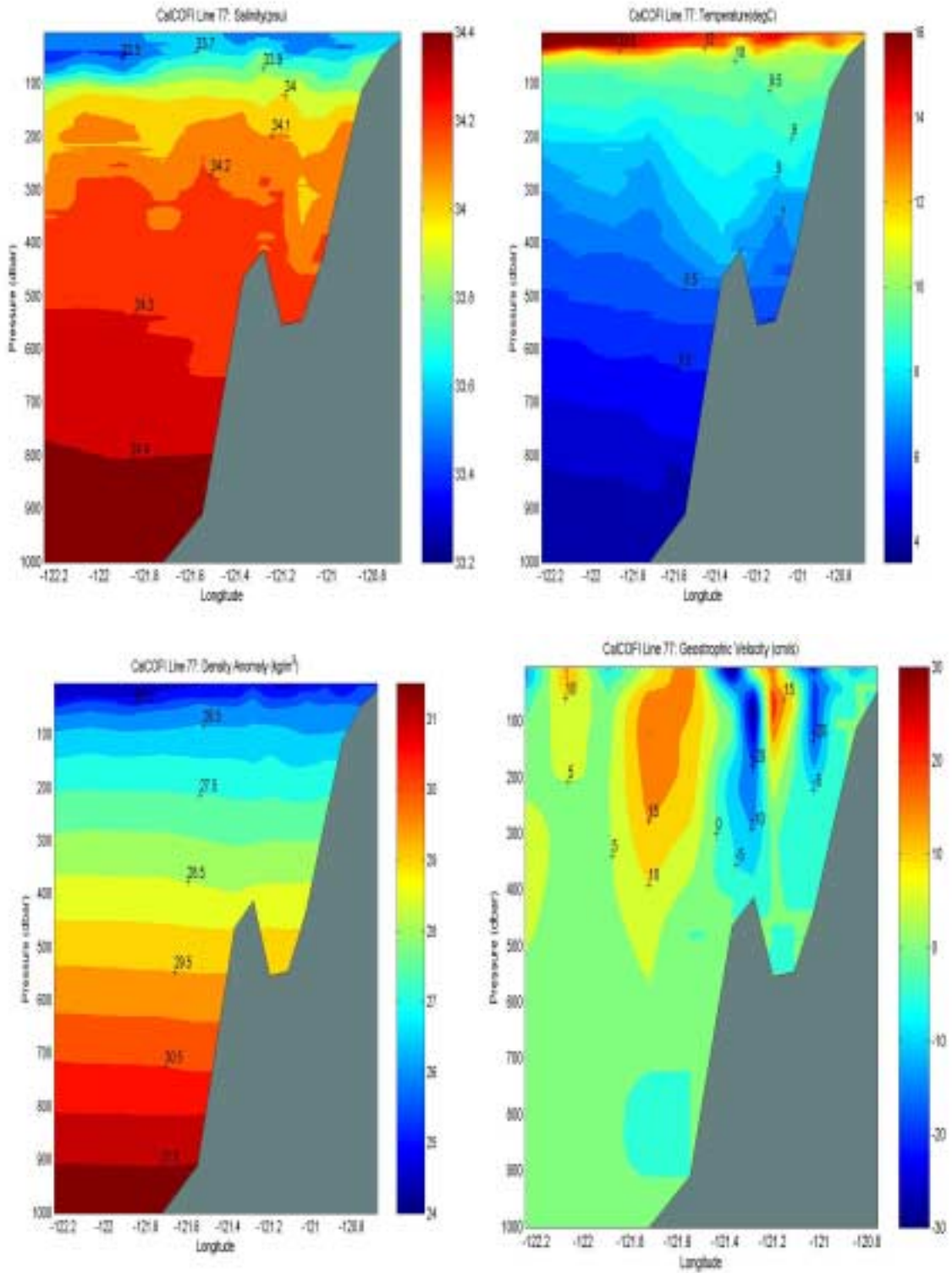


Figure 12
CalCOFI Line 77 – 1000 dbar

Volume Transport Calculations
(using geostrophic velocities)

CaICOFI Line 67

Stations	Distance (km)	Distance (cm)	GV(cm/s)	Depth (m)	Depth (cm)	Vol. Trans (cm ³ /s)	Vol. Trans (m ³ /s)	Vol. Trans (Sv)
# 18-17	18.30	1.83E+06	11.20	300	3.00E+04	6.15E+11	6.15E+06	0.61
# 17-16	18.60	1.86E+06	-1.00	300	3.00E+04	-5.58E+10	-5.58E+04	-0.06
# 16-15	17.70	1.77E+06	-2.10	300	3.00E+04	-1.12E+11	-1.12E+05	-0.11
# 15-14	19.00	1.90E+06	1.10	300	3.00E+04	6.27E+10	6.27E+04	0.06
# 14-13	18.60	1.86E+06	11.90	300	3.00E+04	6.84E+11	6.84E+05	0.69
# 13-12	26.60	2.66E+06	10.00	300	3.00E+04	7.98E+11	7.98E+05	0.80
# 12-11	11.90	1.19E+06	-1.30	300	3.00E+04	-4.64E+10	-4.64E+04	-0.05
# 11-10	19.40	1.94E+06	-6.80	300	3.00E+04	-3.84E+11	-3.84E+06	-0.38
# 10-9	15.70	1.57E+06	-4.40	275	2.75E+04	-1.90E+11	-1.90E+05	-0.19
								1.35

CaICOFI 70s Line

Stations	Distance (km)	Distance (cm)	GV(cm/s)	Depth (m)	Depth (cm)	Vol. Trans (cm ³ /s)	Vol. Trans (m ³ /s)	Vol. Trans (Sv)
# 18-19	18.60	1.86E+06	5.31	300	3.00E+04	2.96E+11	2.96E+06	0.30
# 19-20	18.10	1.81E+06	-2.39	300	3.00E+04	-1.30E+11	-1.30E+05	-0.13
# 20-21	18.60	1.86E+06	10.35	300	3.00E+04	5.78E+11	5.78E+05	0.58
# 21-22	18.20	1.82E+06	-5.60	300	3.00E+04	-3.06E+11	-3.06E+05	-0.31
# 22-23	18.40	1.84E+06	1.06	300	3.00E+04	5.85E+10	5.85E+04	0.06
# 23-24	18.30	1.83E+06	5.81	300	3.00E+04	3.19E+11	3.19E+05	0.32
# 24-25	18.40	1.84E+06	-0.45	300	3.00E+04	-2.48E+10	-2.48E+04	-0.02
# 25-26	18.50	1.85E+06	-2.84	300	3.00E+04	-1.56E+11	-1.56E+05	-0.16
# 26-27	18.20	1.82E+06	-6.55	300	3.00E+04	-3.58E+11	-3.58E+05	-0.36
# 27-28	18.50	1.85E+06	-0.31	300	3.00E+04	-1.72E+10	-1.72E+04	-0.02
# 28-29	18.50	1.85E+06	-1.35	300	3.00E+04	-7.49E+10	-7.49E+04	-0.07
# 29-31	20.60	2.06E+06	1.80	300	3.00E+04	1.11E+11	1.11E+05	0.11
								0.29

Note: "+" Volume transport is to the north on line 67, and west on line 77 ("out" of the box)

Figure 13
Volume Transport Calculations

Volume Transport Calculations
(using geostrophic velocities)

CalCOFI Line 77

Stations	Distance (km)	Distance (cm)	GV(cm/s)	Depth (m)	Depth (cm)	Vol. Trans (cm ³ /s)	Vol. Trans (m ³ /s)	Vol. Trans (Sv)
# 31-30	18.50	1.85E+06	5.95	300	3.00E+04	3.30E+11	3.30E+06	0.3302
# 30-32	18.40	1.84E+06	4.27	300	3.00E+04	2.36E+11	2.36E+05	0.2357
# 32-33	18.30	1.83E+06	4.21	300	3.00E+04	2.31E+11	2.31E+05	0.2311
# 33-34	22.70	2.27E+06	14.15	300	3.00E+04	9.64E+11	9.64E+05	0.9636
# 34-35	14.80	1.48E+06	8.58	300	3.00E+04	3.81E+11	3.81E+05	0.3810
# 35-36	9.40	9.40E+05	-4.69	300	3.00E+04	-1.32E+11	-1.32E+05	-0.1323
# 36-37	9.00	9.00E+05	-5.45	300	3.00E+04	-1.47E+11	-1.47E+05	-0.1472
# 37-38	9.10	9.10E+05	1.51	300	3.00E+04	4.12E+10	4.12E+04	0.0412
# 38-39	9.10	9.10E+05	-3.39	300	3.00E+04	-9.25E+10	-9.25E+04	-0.0925
# 39-40	9.30	9.30E+05	-0.19	267	2.67E+04	-4.72E+09	-4.72E+03	-0.0047
# 40-41	9.40	9.40E+05	0.05	55	5.50E+03	2.59E+08	2.59E+02	0.0003
# 41-42	9.10	9.10E+05	0.06	22	2.20E+03	1.20E+08	1.20E+02	0.0001
# 42-43	8.70	8.70E+05	-0.07	7	7.00E+02	-4.28E+07	-4.28E+01	-0.0000
								1.81

Total volume transport into "box": **1.81 Sv** (North transport on CalCOFI Line 77)

Total volume transport out of "box": **1.35 Sv** (North transport on CalCOFI Line 67)
0.29 Sv (West transport on 70s CalCOFI Line)
1.55 Sv

Difference between volume transport into and out of "box": **0.16 Sv**
(based upon Conservation of Volume)

Figure 13 (continued)

REFERENCES

- Collins, C.A., R.G. Paquette and S.R. Ramp, 1996b. Annual Variability of ocean currents at 350 m depth over the continental slope off Point Sur, California. *CalCOFI rep.*, 37, 257-263.
- Colorado Center for Astrodynamics Research, "Global Near Real-Time Altimeter Data Viewer" (http://www-ccar.colorado.edu/~realtime/global-real-time_ssh/).
- Hickey, B.M., 1979. The California Current System – hypotheses and facts, *Prog. Oceanogr.*, 8, pp. 191-279.
- Hickey, B., "Coastal Oceanography of Western North America from the Tip of Baja California to Vancouver Island; Coastal Segment" in *The Sea*, Robinson, A.R., and Brink, K. H., pp 12,947-12,966, 1998.
- Huyer, A. and R.L. Smith, 1974. A subsurface ribbon of cool water over the continental shelf off Oregon. *J. Phys. Oceanogr.*, 4, 381-391.
- Huyer, A., P.M. Kosro, S.J. Lentz, and R.C. Beardsley, 1989. Poleward flow in the California Current System, in *Poleward Flows along Eastern Oceanic Boundaries*, Coastal and Estuarine Studies No. 34, pp 142-156, Springer-Verlag New York Inc.
- Lien, R.C., M.C. Gregg, "Observations of Turbulence in a Tidal Beam Across a Coastal Ridge", will appear in *J. Geophys. Res.*, 2001.
- Lynn, R.J., and J.J. Simpson, 1987. The California Current System: The seasonal variability of its physical characteristics, *J. Geophys. Res.*, 92, 12,947-12,966.
- Parrish, R.H., Bakun, A., Husby, D.M., and C.S. Nelson, 1983. Comparative climatology of selected environmental processes in relation to eastern boundary current pelagic fish reproduction. in *Proceedings of the expert consultation to examine changes in abundance and species composition of neritic fish resources*. pp 731-778, ed. by G.D. Sharp and J. Csirke. FAO Fish Rep. 291.FAO.
- Pavlova, Y.V., 1966. Seasonal variations of the California Current. *Oceanology*, 6, 806-814.
- Pickard, G.L., and W.J. Emery, 1982. *Descriptive Physical Oceanography; An Introduction*, 5th Ed., pp 64-65, Butterworth/Heinemann.
- Pond, S., and G.L. Pickard, 1983. *Introductory Dynamical Oceanography*, 2nd Ed., pp 66-82, Butterworth/Heinemann.
- Reid, J.L., and R.A. Schwartzlose, 1962. Direct measurements of the Davidson Current off central California, *J. Geophys. Res.*, 67, 2491-2497.